

**Swift-Hohenberg equation with third-order dispersion for optical fiber resonators**

A. Hariz, L. Bahloul, and L. Cherbi

*Laboratoire d'instrumentation, Université des Sciences et de la Technologie Houari Boumediene (USTHB), Bab Ezzouar, Algeria*

K. Panajotov

*Vrije Universiteit Brussel, Department of Applied Physics & Photonics, Pleinlaan 2, B-1050 Brussels, Belgium  
and G. Nadjakov Institute of Solid State Physics, Bulgarian Academy of Sciences, 72 Tzarigradsko Chaussee Blvd., 1784 Sofia, Bulgaria*

M. Clerc and M. A. Ferré

*Departamento de Física and Millennium Institute for Research in Optics, FCFM, Universidad de Chile, Casilla 487-3, Santiago, Chile*

B. Kostet, E. Averlant, and M. Tlidi

*Faculté des Sciences, Université Libre de Bruxelles (ULB), CP.231, Campus Plaine, B-1050 Brussels, Belgium*

(Received 4 December 2018; published 12 August 2019)

We investigate the dynamics of a ring cavity made of photonic crystal fiber and driven by a coherent beam working near to the resonant frequency of the cavity. By means of a multiple-scale reduction of the Lugiato-Lefever equation with high-order dispersion, we show that the dynamics of this optical device, when operating close to the critical point associated with bistability, is captured by a real order parameter equation in the form of a generalized Swift-Hohenberg equation. A Swift-Hohenberg equation has been derived for several areas of nonlinear science such as chemistry, biology, ecology, optics, and laser physics. However, the peculiarity of the obtained generalized Swift-Hohenberg equation for photonic crystal fiber resonators is that it possesses a third-order dispersion. Based on a weakly nonlinear analysis in the vicinity of the modulational instability threshold, we characterize the motion of dissipative structures by estimating their propagation speed. Finally, we numerically investigate the formation of moving temporal localized structures often called cavity solitons.

DOI: [10.1103/PhysRevA.100.023816](https://doi.org/10.1103/PhysRevA.100.023816)**I. INTRODUCTION**

The control of linear and nonlinear properties of photonic crystal fibers (PCF) has led to several applications in optoelectronics, sensing, and laser science (see recent overview on this issue [1] and references therein). The improvement of the fabrication capabilities of high-quality integrated microstructured resonators such as ring, microring, microdisk, or Fabry-Pérot cavities are drawing considerable attention from both fundamental and applied points of view. Among those, an important class is the photonic crystal fiber resonators where high-order chromatic dispersion could play an important role in the dynamics [2,3], particularly in relation with supercontinuum generation [4,5]. On the other hand, driven optical microcavities are widely used for the generation of optical frequency combs. They can be modeled by the Lugiato-Lefever equation [6] that possesses solutions in the form of localized structures (LSs) [7,8]. Optical frequency combs generated in high- $Q$  Kerr resonators [9] are in fact the spectral content of the stable temporal pattern occurring in the cavity. Among the possible dissipative structures, the temporal localized structures often called dissipative solitons appear in the form of a stable single pulse on top of a low background. They have been theoretically predicted in [7] and experimentally observed in [8]. The link between temporal localized structures and Kerr comb generation in high- $Q$  resonators has motivated further interest in this issue.

When inserting a photonic crystal fiber in a cavity which is driven by a continuous beam, the light inside the fiber is coherently superimposed with the input beam at each round trip. The nonlinear Schrödinger equation supplemented by the cavity boundary condition leads to a generalized Lugiato-Lefever equation (LLE) [10]. The inclusion of the fourth-order dispersion allows the modulational instability (MI) to have a finite domain of existence delimited by two pump power values [10], as well as to stabilize dark temporal LSs [11–13]. In the absence of fourth-order dispersion, with only second or/and third orders of dispersion, front interaction leads to the formation of moving LS in a regime far from any modulational instability [14]. An analytical study of the interaction between LSs under the action of Cherenkov radiation or dispersive waves has been conducted in [15]. In addition, it has been shown that the interference between the dispersive waves emitted by the two interacting LSs produces an oscillating pattern responsible for the stabilization of the bound states. A derivation of equations governing the time evolution of the position of two well-separated LSs interacting weakly via their exponentially decaying tails has been presented in [15].

In this paper, we derive a Swift-Hohenberg equation (SHE) with third-order dispersion describing the evolution of pulses propagating in a photonic crystal fiber resonator. This reduction is performed for small-frequency modes and close to a second-order critical point marking the onset of a hysteresis

loop (nascent bistability). The dimensionless generalized real SHE reads

$$\frac{\partial \phi}{\partial t} = y + c\phi - \phi^3 + \beta \frac{\partial^2 \phi}{\partial \tau^2} + \beta' \frac{\partial^3 \phi}{\partial \tau^3} - \frac{\partial^4 \phi}{\partial \tau^4}. \quad (1)$$

Here  $\phi(t, \tau)$  is the deviation of the electric field from its value at the onset of bistability. The variable  $\phi$  is a scalar real field. The time variable  $t$  corresponds to the slow evolution of  $\phi$  over successive round trips.  $\tau$  accounts for the fast dynamics that describes how the electric-field envelope changes along the fiber. The parameters  $y$  and  $c$  are deviations of the amplitude of the injected field and the cavity detuning from their critical values at the onset of the modulational instability, respectively. The coefficients  $\beta$  and  $\beta'$  account for second- and third-order chromatic dispersion, respectively. Without loss of generality, we rescale the fourth-order dispersion coefficient and the cubic coefficient to unity. The third and the fourth orders of dispersion are usually neglected in fiber cavity models [6]. However, the dispersion characteristics of photonic crystal resonators impose to consider high-order dispersion [16–18].

The paper is organized as follows. After an introduction, we present the Lugiato-Lefever equation with high-order dispersion, and we perform a linear stability analysis of the homogeneous steady states in Sec. II. In Sec. III, we derive a generalized real Swift-Hohenberg equation. A weakly nonlinear analysis of the real Swift-Hohenberg equation is presented in Sec. IV. In this section, we also present a derivation of their linear and nonlinear velocities. Moving temporal localized structures with a single peak or more peaks are demonstrated in Sec. V. Section VI presents a comparison between the generalized LLE and the derived SHE models. In the limit of small third-order dispersion, an analytical expression for the speed of the localized structure is provided in Sec. VII. We conclude in Sec. VIII.

## II. LUGIATO-LEFEVER EQUATION WITH HIGHER-ORDER DISPERSIONS

We consider an optical cavity with a length  $L$  filled with a photonic crystal fiber, and synchronously pumped by a coherent injected beam, as described in Fig. 1. A continuous wave  $E_i$  is injected into the cavity by means of a beam splitter. The field  $E$  propagates inside the fiber and experiences dispersion, Kerr effect, and dissipation. We neglect the Raman scattering effect by assuming that the Kerr time response of fiber is instantaneous. Indeed, when the pulse width is larger than 1 ps, the Raman response can be neglected as discussed in [19].

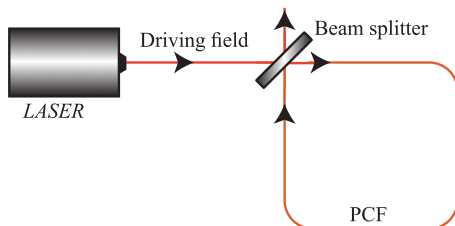


FIG. 1. Schematic representation of a ring cavity filled with a photonic crystal fiber (PCF) and driven by a coherent beam.

The linear phase shift accumulated during one cavity round trip is denoted by  $\Phi_0$ . The intensity mirror transmissivity (reflectivity) is  $T^2$  ( $R^2$ ). The second-, third-, and fourth-order dispersion terms are, respectively,  $\beta_{2,3,4}$ .  $\tau$  is the time in the reference frame moving at the group velocity of the light describing the fast evolution of the field envelope within the cavity;  $\tau \equiv \tau(T^2/L)^{1/2}$ . The time  $t$  describes the slow evolution of the field envelope between two consecutive cavity round trips and is scaled such that the decay rate is unity, i.e.,  $t \equiv tT^2/2t_r$ , where  $t_r$  is the round trip time. The normalized intracavity field is  $E \equiv E\sqrt{2\gamma L/T^2}$  and the injected field is  $S = 2/T(2\gamma L/T^2)^{1/2}E_i$ , with  $\gamma$  the nonlinear coefficient. The normalized cavity detuning is  $\theta = 2\Phi_0/T^2$ . We also replace the coefficients  $\beta_{2,3,4}$  by  $\beta$  and  $\beta'$  through the relations  $\partial/\partial\tau \equiv \beta_4^{-1/4}\partial/\partial\tau$ ,  $\beta = \beta_2/\sqrt{\beta_4}$ , and  $\beta' = \beta_3/\beta_4^{3/4}$ .

In its dimensionless form, the generalized Lugiato-Lefever equation studied in [10] reads

$$\begin{aligned} \frac{\partial E}{\partial t} = & S - (1 + i\theta)E + i|E|^2E - i\beta \frac{\partial^2 E}{\partial \tau^2} \\ & + \beta' \frac{\partial^3 E}{\partial \tau^3} + i \frac{\partial^4 E}{\partial \tau^4}. \end{aligned} \quad (2)$$

The homogeneous stationary solutions (HSSs)  $E_s$  of Eq. (2) are described by  $S^2 = I_s[1 + (\theta - I_s)^2]$  and  $I_s = |E_s|^2$ . This system will exhibit a bistable behavior for  $\theta > \theta_c = \sqrt{3}$  and a monostable behavior for  $\theta \leq \theta_c$ . The linear stability of the homogeneous steady states has been performed in [10]. The presence of a fourth-order dispersion gives rise to (i) a degenerate modulational instability where two separate frequencies simultaneously appear and (ii) appearance of a second MI that stabilizes the high intensity regime [10]. The linear stability analysis of the homogeneous solutions with respect to finite frequency perturbation of the form  $\exp(i\Omega\tau + \lambda t)$  yields

$$\lambda_{\pm} = -1 - i\beta'\Omega^3 \pm \sqrt{I_s^2 - (\theta - 2I_s - \beta\Omega^2 - \Omega^4)^2}. \quad (3)$$

This dispersion relation through the conditions  $\partial\lambda/\partial\Omega = \partial^2\lambda/\partial\Omega^2 = 0$  yields expressions for the critical frequencies at the first MI bifurcation which are degenerate:

$$\Omega_{l,u}^2 = \frac{-\beta \pm \sqrt{\beta^2 + 4(\theta - 2I_s)}}{2}. \quad (4)$$

These two frequencies ( $\Omega_l$  and  $\Omega_u$ ) are simultaneously and spontaneously generated at the primary threshold  $I_s = I_{1m} = 1$ . When the two critical frequencies  $\Omega_{l,u}$  are close to each other, it has been shown that intrinsic beating frequencies  $\Omega_l \pm \Omega_u$  appear [20]. Besides this first degenerate modulational instability, the fourth-order dispersion allows for the stabilization of the high intensity regime by creating another MI. The critical value of the frequency at the upper bifurcation point  $I_{2m}$  is given by  $\Omega_c^2 = -\beta/4$ . It is then possible to restabilize the stationary state by driving the system to the large intensity regime ( $I > I_{2m}$ ).

### III. GENERALIZED SWIFT-HOHENBERG EQUATION FOR PHOTONIC CRYSTAL FIBER RESONATORS

#### Derivation of a generalized Swift-Hohenberg equation

The purpose of this section is to present the derivation of the generalized Swift-Hohenberg for a photonic crystal fiber resonator. For this purpose, we use the multiple scale method. To this aim, we explore the space-time dynamics in the vicinity of the critical point associated with the nascent bistability. More precisely, for  $\theta = \theta_c$ , there exists a second-order critical point marking the onset of a hysteresis loop. This transition point is defined by  $\partial S/\partial I_s = \partial^2 S/\partial I_s^2 = 0$ . The coordinates of this critical point are

$$E_c = \left( \frac{3}{4} - i \frac{\sqrt{3}}{4} \right) S_c, \quad S_c^2 = \frac{8\sqrt{3}}{9}. \quad (5)$$

We decompose the electrical field in real and imaginary parts as  $E = X_1 + iX_2$ , replace it in Eq. (2), and get

$$\begin{aligned} \frac{\partial X_1}{\partial t} &= S - X_1 + \theta X_2 - X_2 X_1^2 - X_2^3 \\ &\quad + \beta \frac{\partial^2 X_2}{\partial \tau^2} + \beta' \frac{\partial^3 X_1}{\partial \tau^3} - \frac{\partial^4 X_2}{\partial \tau^4}, \end{aligned} \quad (6)$$

$$\begin{aligned} \frac{\partial X_2}{\partial t} &= -X_2 - \theta X_1 + X_1 X_2^2 + X_1^3 \\ &\quad - \beta \frac{\partial^2 X_1}{\partial \tau^2} + \beta' \frac{\partial^3 X_2}{\partial \tau^3} + \frac{\partial^4 X_1}{\partial \tau^4}. \end{aligned} \quad (7)$$

We introduce the excess variables  $U$  and  $V$ :  $X_1(\tau, t) = x_{1s} + U(\tau, t)$  and  $X_2(\tau, t) = x_{2s} + V(\tau, t)$  with  $x_{1s}$  and  $x_{2s}$  being, respectively, the real and imaginary parts of the homogeneous stationary solution given by

$$S - x_{1s} + \theta x_{2s} - x_{2s} x_{1s}^2 - x_{2s}^3 = 0, \quad (8)$$

$$-x_{2s} - \theta x_{1s} + x_{1s} x_{2s}^2 + x_{1s}^3 = 0. \quad (9)$$

At the critical point associated with bistability, the real and imaginary parts are  $x_{1c} = 3S_c/4$  and  $x_{2c} = -\sqrt{3}S_c/4$  [cf. Eq. (5)]. In order to explore the vicinity of the nascent hysteresis, we introduce a small parameter  $\epsilon$  which measures the distance from the critical point associated with bistability

$$\theta = \sqrt{3} + \epsilon^2 \delta. \quad (10)$$

Indeed,  $\delta$  accounts for the separation of detuning with respect to the critical one. We then expand in powers of  $\epsilon$  the excess variables and the injected field as

$$U = \epsilon u_0 + \epsilon^2 u_1 + \epsilon^3 u_2 + \dots, \quad (11)$$

$$V = \epsilon v_0 + \epsilon^2 v_1 + \epsilon^3 v_2 + \dots, \quad (12)$$

$$S = S_c + \epsilon S_1 + \epsilon^2 S_2 + \epsilon^3 S_3 + \dots, \quad (13)$$

and also introduce the slow and the fast time scales,  $t \equiv t/\epsilon^2$  and  $\tau \equiv \tau/\sqrt{\epsilon}$ . A preliminary analysis indicates that we need to consider that  $\beta$  is small  $\beta \equiv \epsilon \beta$ . This is because we consider a low-frequency (or large period) regime. In this way, the MI instability threshold is close to the critical point. We now replace all the above scalings and expansions in Eq. (6)

and Eq. (7), and make an expansion in series of  $\epsilon$  up to the order  $\epsilon^3$ . To  $O(\epsilon)$ , one gets

$$\begin{pmatrix} S_1 \\ 0 \end{pmatrix} = \begin{bmatrix} 1 + 2x_{1c}x_{2c} & x_{1c}^2 + 3x_{2c}^2 - \theta_c \\ -x_{2c}^2 - 3x_{1c}^2 + \theta_c & 1 - 2x_{1c}x_{2c} \end{bmatrix} \begin{pmatrix} u_0 \\ v_0 \end{pmatrix}.$$

By replacing the values of  $\theta_c$  and  $x_{1c,2c}$  in these equations, the solvability condition yields  $S_1 = 0$  and  $u_0(\tau, t) = \sqrt{3}v_0(\tau, t)$ . To the next order  $O(\epsilon^2)$ , we obtain

$$\begin{aligned} &\begin{bmatrix} 1 + 2x_{1c}x_{2c} & x_{1c}^2 + 3x_{2c}^2 - \theta_c \\ -x_{2c}^2 - 3x_{1c}^2 + \theta_c & 1 - 2x_{1c}x_{2c} \end{bmatrix} \begin{pmatrix} u_1 \\ v_1 \end{pmatrix} \\ &= \begin{pmatrix} s_2 + x_{2c}\delta \\ -x_{1c}\delta \end{pmatrix} + \begin{pmatrix} -x_{2c}u_0^2 - 3x_{2c}v_0^2 - 2x_{1c}u_0v_0 \\ x_{1c}v_0^2 + 3x_{1c}u_0^2 + 2x_{2c}u_0v_0 \end{pmatrix}. \end{aligned}$$

In these equations, we replace the values of  $\theta_c$ ,  $x_{1c,2c}$ ,  $S_1 = 0$ ,  $u_0(\tau, t) = \sqrt{3}v_0(\tau, t)$ , and the solvability condition leading to

$$S_2 = \frac{\delta}{2^{1/2}3^{1/4}}, \quad (14)$$

$$u_1 = \sqrt{3}v_1 + \left( \frac{3}{4} \right)^{3/4} \delta - 2^{3/2}3^{-1/2}u_0^2.$$

Finally, to the next order  $O(\epsilon^3)$ , through the solvability condition, we get

$$\sqrt{3} \frac{\partial u_0}{\partial t} = \sqrt{3}S_3 - \frac{4}{3}u_0^3 + \delta u_0 + \beta \frac{\partial^2 u_0}{\partial \tau^2} + \sqrt{3}\beta' \frac{\partial^3 u_0}{\partial \tau^3} - \frac{\partial^4 u_0}{\partial \tau^4}. \quad (15)$$

Introducing the following change of variables and parameters  $\phi \equiv vu_0$ ,  $y \equiv \sqrt{3}S_3$ ,  $c \equiv (\delta/v)$ ,  $t \equiv (vt/\sqrt{3})$ ,  $\beta \equiv v\beta$ , and  $\tau \equiv v\tau$ , with  $v = (4/3)^{1/3}$ , we obtain the real Swift-Hohenberg equation with the third-order dispersion

$$\frac{\partial \phi}{\partial t} = y + c\phi - \phi^3 + \beta \frac{\partial^2 \phi}{\partial \tau^2} + \beta' \frac{\partial^3 \phi}{\partial \tau^3} - \frac{4}{3} \frac{\partial^4 \phi}{\partial \tau^4}. \quad (16)$$

Trivially, by normalizing the time  $\tau$ , and the dispersion coefficients, we recover Eq. (1). The SHE is a well-known paradigm in the study of pattern formation and localized structures. Generically, it applies to systems that undergo a symmetry breaking modulational instability (often called Turing instability [6]) close to the critical point associated with bistability (nascent optical bistability). It has been derived first under these conditions in hydrodynamics [21], and later on in chemistry [22], plant ecology [23], and nonlinear optics [24,25]. Other real order parameter equations in the form of nonvariational Swift-Hohenberg model have been also derived for spatially extended systems [26].

In the absence of the third-order dispersion, the Swift-Hohenberg equation (16) is variational, i.e., there exists a Lyapunov functional guaranteeing that evolution proceeds towards the state for which the functional has the smallest possible value which is compatible with the system boundary conditions. Without the third-order dispersion in the Swift-Hohenberg model Eq. (16), localized structures do not move. However, when a nonvariational term such as  $\phi \partial^2 \phi / \partial \tau^2$  is considered, localized structures can become propagative [27]. The conditions under which periodic patterns and localized structures appear are closely related. Dynamically speaking, a subcritical modulational instability underlies the pinning

phenomena responsible for the generation of temporal localized structures [28].

The homogeneous steady states  $\phi_s$  of Eq. (16) satisfy the cubic equation  $y = \phi_s(\phi_s^2 - c)$ . The monostable regime will be for  $c < 0$  and the bistable regime will occur when  $c > 0$ . The linear stability analysis with respect to finite frequency perturbation of the form  $\phi = \phi_s + \delta\phi e^{\lambda t - i\omega\tau} + \text{c.c.}$ , where c.c. denotes the complex conjugate and with  $\delta\phi \ll 1$ , yields the characteristic equation

$$\lambda = c - \beta\omega^2 - i\beta'\omega^3 - \frac{4}{3}\omega^4 - 3\phi_s^2. \quad (17)$$

In the absence of the third-order dispersion, i.e.,  $\beta' = 0$ , the homogeneous steady states undergo a modulational instability at

$$\phi_{M\pm} = \pm\sqrt{\frac{\beta^2}{16} + \frac{c}{3}}, \quad y_{M\pm} = \left(\frac{\beta^2}{16} - \frac{2c}{3}\right)\phi_{M\pm}. \quad (18)$$

At both thresholds associated with MI, the critical frequency is  $\omega_M^2 = -3\beta/8$ .

#### IV. WEAKLY NONLINEAR ANALYSIS

To calculate the nonlinear solutions bifurcating from the threshold associated with modulational instability, we use a weakly nonlinear analysis. To this end, we introduce an excess variable as  $\phi \equiv \phi_s + \psi$ . We expand  $\phi_s$ ,  $\psi$ , and  $y$  in terms of a small parameter  $\mu$  that measures the distance from the modulational instability threshold:

$$\begin{aligned} \phi_s &= \phi_{M\pm} + \mu\phi_1 + \mu^2\phi_2 + \mu^3\phi_3 + \dots, \\ \psi &= \mu\psi_1 + \mu^2\psi_2 + \mu^3\psi_3 + \dots, \\ y &= y_{M\pm} + \mu y_1 + \mu^2 y_2 + \mu^3 y_3 + \dots. \end{aligned} \quad (19)$$

The coordinates of the thresholds associated with the modulational instability  $\phi_{M\pm}$  and  $y_{M\pm}$  are explicitly given by Eq. (18). We introduce a slow time

$$\frac{\partial}{\partial t} = \frac{\partial}{\partial t_1} + \mu^2 \frac{\partial}{\partial t_2}. \quad (20)$$

The solution to the homogeneous linear problem obtained at the leading order in  $\mu$  is

$$\psi_1 = W \exp[i(\omega_M\tau + \kappa t_1)] + \text{c.c.} \quad (21)$$

The quantities  $\psi_i$  and  $\phi_i$  ( $i = 1, 2$ ) can be calculated by inserting Eqs. (19) into the real Swift-Hohenberg Eq. (16) and equating terms with the same powers of  $\mu$ .

At third order in  $\mu$ , the solvability condition yields the following amplitude equation:

$$\partial A / \partial t = -6\alpha A + (f + ig)|A|^2 A, \quad (22)$$

where  $A = \mu W$ ,  $\alpha = \phi_s - \phi_{M\pm}$  measures the distance from the second instability threshold, and

$$\begin{aligned} f &= \left[ \frac{36\phi_{M\pm}^2 (\frac{27}{8}\beta^2)}{\frac{729}{64}\beta^4 + 256\kappa^2} + \frac{192}{\beta^2}\phi_{M\pm}^2 - 3 \right], \\ g &= \frac{576\phi_{M\pm}^2\kappa}{\frac{729}{64}\beta^4 + 256\kappa^2}. \end{aligned} \quad (23)$$

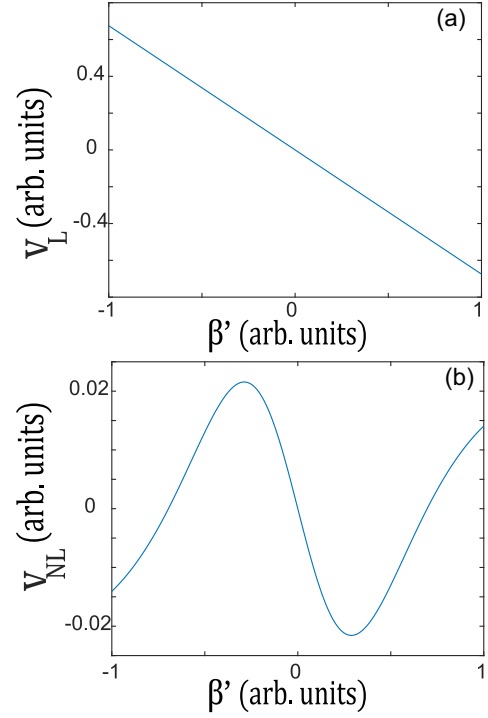


FIG. 2. Linear (a) and nonlinear (b) speed as a function of the parameter  $\beta'$  computed from Eqs. (26) for  $\beta = -0.6$  and  $c = -0.06$ .

The amplitude equation (22) admits the following solution:  $A = |A| \exp[i(qt + \omega_M\tau)]$ . The third-order dispersion adds a new nonlinear phase  $q$ . By replacing this solution in Eq. (22), we obtain

$$|A|^2 = 6 \frac{\phi_s - \phi_{M\pm}}{f}, \quad q = g|A|^2. \quad (24)$$

The nonlinear phase  $q$  is caused by the third-order dispersion. When taking into account the nonlinear correction, the velocity takes the following form:

$$v = v_L + v_{NL}, \quad (25)$$

where the linear and the nonlinear velocities are

$$v_L = \frac{\partial \text{Im}(\lambda)}{\partial \omega_M} = -3\beta'\omega^2, \quad v_{NL} = \frac{\partial q}{\partial \omega_M}. \quad (26)$$

In the linear regime, the critical frequency, as well as the threshold associated with modulational instability, are not affected by the third-order dispersion. The linear and nonlinear speeds as a function of the parameter  $\beta'$  are shown in Fig. 2 for  $\beta = -0.6$  and  $c = -0.06$ . In the absence of the third-order dispersion, the transition from super- to subcritical modulational instability occurs when  $c = c_{\text{sub}} = -87\beta^2/38$  [29]. The modulational bifurcation is subcritical when  $c > c_{\text{sub}}$ . The subcritical nature of the bifurcation can occur even in the monostable regime  $c_{\text{sub}} < c < 0$ .

#### V. MOVING TEMPORAL LOCALIZED STRUCTURES

Examples of a single, two, or three peaks stationary symmetric temporal localized structures are shown in Figs. 3–5. They have been obtained numerically by using a periodic boundary condition compatible with the ring geometry of the

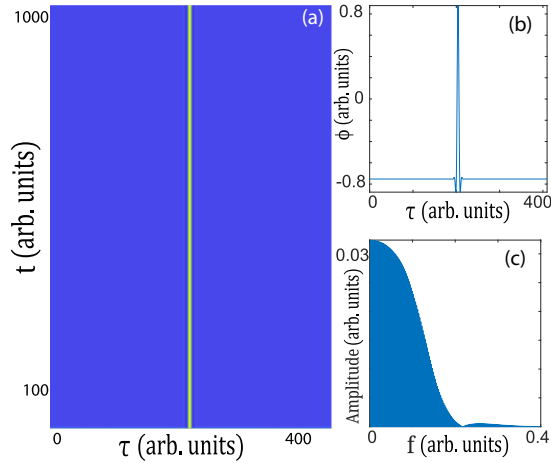


FIG. 3. Space-time map (a) and temporal profile (b) of one localized structure, integrated for 1024 cells,  $c = 0.5$ ,  $y = -0.05$ ,  $\beta = -1$ , and  $\beta' = 0$ . Panel (c) shows the corresponding Fourier spectra, calculated using the integration of 500 round trips in the cavity.

optical resonator depicted in Fig. 1. However, the third-order dispersion breaks the reflection symmetry and allows for the motion of localized structures. Examples of a single, two, or three peaks moving temporal localized structures are shown in Figs. 6–8. The frequency resolution for the discrete Fourier transform is proportional to the sample rate and inversely proportional to the length of the time series. We increase the frequency resolution by increasing the length of our time series, i.e., by taking 500 round trips in the cavity [30].

Localized structures occur in the regime where the homogeneous steady state coexists with a spatially periodic structure. In addition, the system exhibits a high degree of multistability in a finite range of the control parameter values often called the pinning region [31]. The number of LSs and their temporal distribution along the longitudinal direction

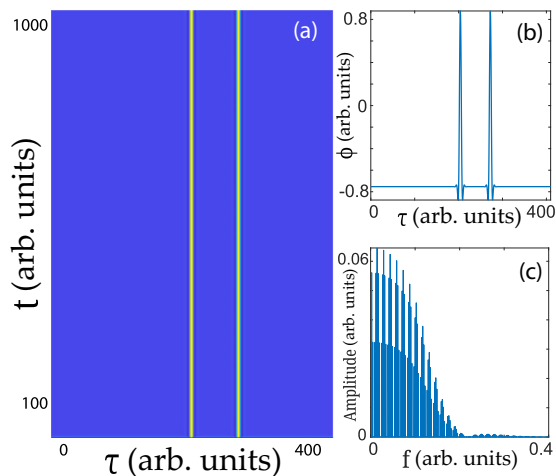


FIG. 4. Space-time map (a) and temporal profile (b) of two localized structures, integrated for 1024 cells,  $c = 0.5$ ,  $y = -0.05$ ,  $\beta = -1$ , and  $\beta' = 0$ . Panel (c) shows the corresponding Fourier spectra, calculated using the integration of 500 round trips in the cavity.

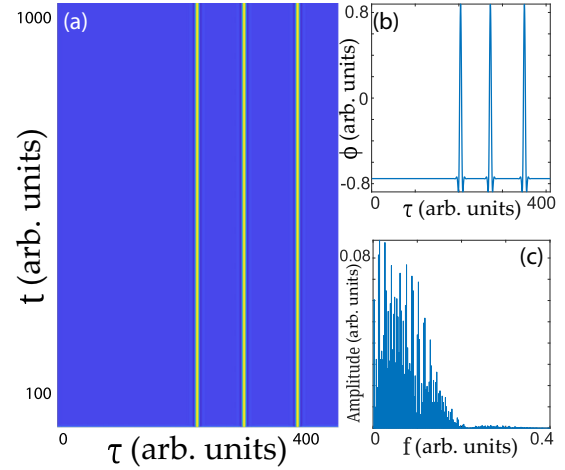


FIG. 5. Space-time map (a) and temporal profile (b) of three localized structures, integrated for 1024 cells,  $c = 0.5$ ,  $y = -0.05$ ,  $\beta = -1$ , and  $\beta' = 0$ . Panel (c) shows the corresponding Fourier spectra, calculated using the integration of 500 round trips in the cavity.

within the cavity are determined by the initial conditions [28]. Two or more localized structures interact through their overlapping oscillatory tails when they are close to one another. In the case where  $\beta' = 0$ , an analytical expression of the potential that describes such interaction in the case of weak overlap is derived in [32].

The interaction between the LSs then leads to the formation of clusters or LS complexes. Dissipative structures have been observed in all areas of nonlinear science, such as chemistry, biology, ecology, optics, and physics (see recent overview on this issue [33,34]).

A quantitative comparison between the stationary and moving LS obtained from the SHE and from the LLE will be discussed in the next section.

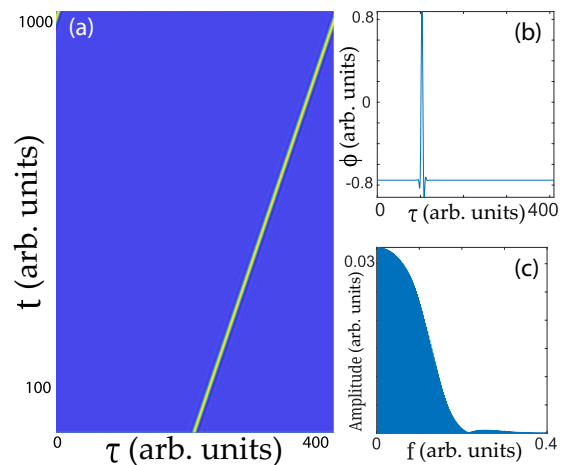


FIG. 6. Space-time map (a) and temporal profile (b) of one localized structure, integrated for 1024 cells,  $c = 0.5$ ,  $y = -0.05$ ,  $\beta = -1$ , and  $\beta' = 0.5$ . Panel (c) shows the corresponding Fourier spectra, calculated using the integration of 500 round trips in the cavity.

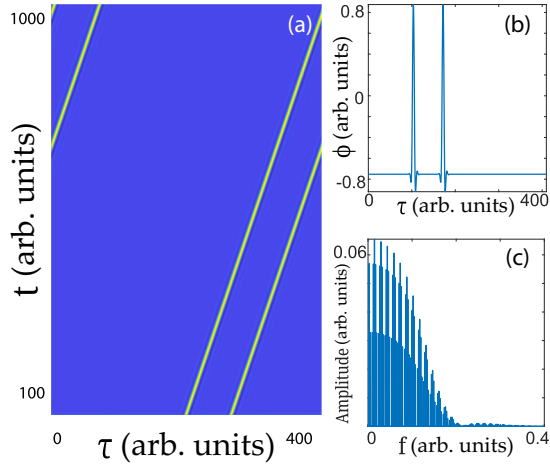


FIG. 7. Space-time map (a) and temporal profile (b) of two localized structures, integrated for 1024 cells,  $c = 0.5$ ,  $y = -0.05$ ,  $\beta = -1$ , and  $\beta' = 0.5$ . Panel (c) shows the corresponding Fourier spectra, calculated using the integration of 500 round trips in the cavity.

## VI. COMPARISON BETWEEN THE LLE AND THE SHE MODELS

The real order parameter description leading to the derivation of a Swift-Hohenberg equation is rather generic and it is a well-known paradigm in the study of spatial periodic or localized patterns. Generically, it applies to systems that undergo a symmetry-breaking instability close to a second-order critical point marking the onset of a hysteresis loop (nascent bistability). The reduction from the generalized LLE to a SHE type of model equation with a third dispersion has been performed in Sec. III A. The SHE captures several behaviors of the LLE such as optical bistability, modulational instability, and moving localized structures.

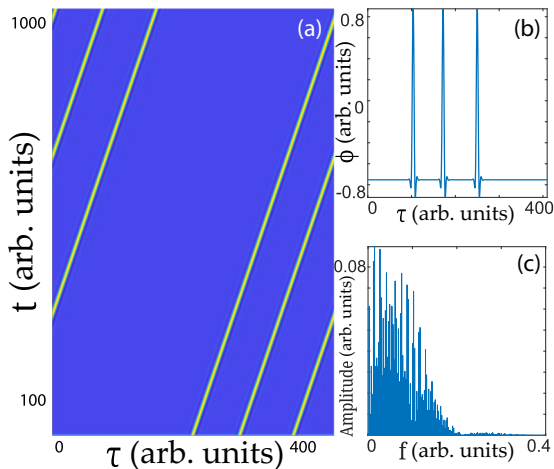


FIG. 8. Space-time map (a) and temporal profile (b) of three localized structures, integrated for 1024 cells,  $c = 0.5$ ,  $y = -0.05$ ,  $\beta = -1$ , and  $\beta' = 0.5$ . Panel (c) shows the corresponding Fourier spectra, calculated using the integration of 500 round trips in the cavity.

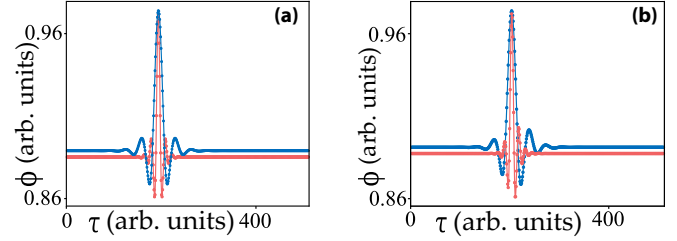


FIG. 9. Comparison of profiles obtained from the Lugiato-Lefever model (dark blue) and from the Swift-Hohenberg model (light red). Parameters are  $\theta = 1.73196$ ,  $S = 1.2407$ ,  $\beta = 0.145$  for the LL model,  $y = 0.0578245$ ,  $c = -0.00630608$ ,  $\beta = 1.15$  for the SH model, and for both (a) motionless localized structures obtained for  $\beta' = 0$  and (b) traveling localized structures obtained for  $\beta' = 0.04$ .

In order to perform a quantitative comparison between the LLE and a SHE, we fix the detuning parameter to  $\theta = 1.73196$ . In this case, the transmitted intensity as a function of the input intensity is bistable. The distance from this critical point is provided by Eq. (10). This equation fixes the value of  $\epsilon = 0.12$  for  $\delta = -0.00573$ . The relation between injected field  $S$  in the LLE and  $y$  in the SHE is given by Eq. (13), with  $S_1 = 0$  and  $S_2 = \delta/(2^{1/2}3^{1/4})$  [cf. Eq. (14)].  $y \equiv \sqrt{3}S_3$ . This relation reads

$$S = S_c + \frac{\delta}{2^{1/2}3^{1/4}}\epsilon^2 + \epsilon^3 y/\sqrt{3} + \dots \quad (27)$$

The numerical value of the injected field is  $S = 1.2407$ . The values of coefficients of the second derivative in  $\tau$  in the LLE and the SHE are  $\beta = 0.145$  and  $\beta = 1.266$ , respectively. To compare the localized solutions of both models, we use the relation between the real order parameter  $\phi$  and the real part of the intracavity field  $X_1 = \text{Re}(E)$

$$X_1 = x_{1s} + \epsilon \left(\frac{3}{4}\right)^{1/3} \phi + \epsilon^2 \left[ \left(\frac{3}{4}\right)^{5/12} c - 6^{1/6} \phi^2 \right] + \dots \quad (28)$$

The results of the comparison between the numerical simulation of LLE and SHE are shown in Fig. 9. In the absence of the third-order dispersion, the profiles of stationary solutions obtained by numerical simulation of the LLE and the SHE are shown in Fig. 9(a). The gap between the homogeneous domains scales as  $\epsilon^2$ . In the presence of the third-order dispersion, the profiles of moving localized structures are asymmetric. The obtained numerical simulation of the LLE and the SHE are shown in Fig. 9(b). Both profiles (of either stationary or moving localized solutions) demonstrate that the peak intensities and the widths of the LSs calculated by LLE and SHE are in good agreement. Next, we compare the speed of a moving LS obtained from the LLE and the SHE. To do that, we fix all parameters and vary the third-order dispersion coefficient. The results are shown in Fig. 10.

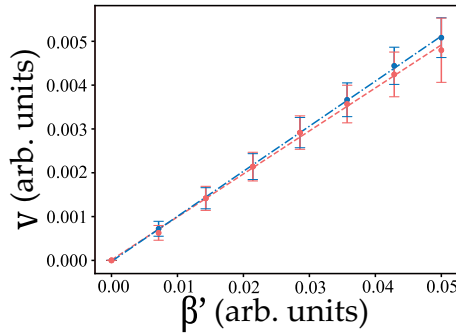


FIG. 10. Comparison of the speed of localized structures obtained from the Lugiato-Lefever model (dark blue) and from the Swift-Hohenberg model (light red). Parameters are  $\theta = 1.73196$ ,  $S = 1.2407$ ,  $\beta = 0.145$  for the LL model and  $y = 0.0578245$ ,  $c = -0.00630608$ ,  $\beta = 1.15$  for the SH model.

### VII. PULSE SOLUTIONS FOR SMALL THIRD-ORDER DISPERSION

Another strategy to understand the effect of the third-order chromatic dispersion is to consider small  $\beta'$ . Damped oscillations towards its flanks characterize the localized structure. Analytical expressions of this motionless solution are not accessible as a consequence of the chaos theory [35]. Let us introduce  $\phi_0(\tau - \tau_0)$  as the localized structure of model (16) with  $\beta' = 0$ , where  $\tau_0$  accounts for the temporal position of the global maximum of the localized structure. Hence the temporal variation of  $\tau_0$  accounts for the speed of moving localized structure. In order to calculate the speed of the LSs, we consider the following ansatz:

$$\phi(t, \tau) = \phi_0[\tau - \tau_0(t)] + w(t, \tau), \quad (29)$$

where  $\tau_0$  is promoting to a temporal variable, which has variation of the order  $\beta'$  [ $\dot{\tau}_0(t) \sim \beta'$ ], and  $w(t, \tau)$  is a small correction function of the order of third chromatic dispersion. Introducing the ansatz (29) in the generalized real Swift-Hohenberg equation (16), linearizing in  $w$ , and imposing the solvability conditions, after straightforward calculations, we obtain

$$\dot{\tau}_0 = v \equiv \beta' \frac{\int \left(\frac{\partial^2 \phi_0}{\partial \tau^2}\right)^2 d\tau}{\int \left(\frac{\partial \phi_0}{\partial \tau}\right)^2 d\tau}. \quad (30)$$

Note that the speed of propagation of the pulse is proportional to the third-order chromatic dispersion. From Eq. (30) we see that, if  $\beta'$  is positive (negative), the localized structure propagates towards the positive (negative) flank. Figure 11 shows a comparison between the analytical expression of the speed of single peak LSs, Eq. (30), and numerical simulations of the governing equation (16). From this figure, we can infer a quite good agreement when  $\beta'$  is small.

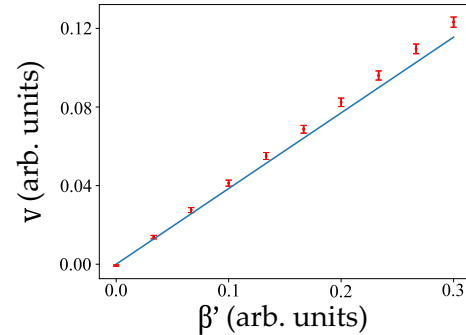


FIG. 11. Localized structure speed as function of  $\beta'$ . Points are obtained from numerical simulations of Eq. (16). The continuous line corresponds to the plot of formula (30). Parameters are  $c = 0.5$ ,  $y = -0.05$ , and  $\beta = -1$ .

### VIII. CONCLUSIONS

Employing a multiple-scale reduction near the bifurcation threshold associated with the modulational instability and close to a second-order critical point marking the onset of a hysteresis loop (nascent bistability), we have derived a real Swift-Hohenberg equation describing the evolution of the envelope of the electric field circulating inside an optical Kerr resonator. The presence of third-order dispersion renders the obtained Swift-Hohenberg equation nonvariational meaning there is no free energy or Lyapunov functional to minimize in the instability problem we have considered. A linear and a weakly nonlinear analysis has been performed to identify the conditions under which a transition from super- to subcritical modulational instability takes place. More importantly, we have shown that the third-order dispersion allows for temporal localized structures to move with a constant speed as a result of the broken reflexion symmetry. We have characterized this motion by estimating the speed associated with it. We have also performed a quantitative comparison between the results obtained from the Lugiato-Lefever model and the Swift-Hohenberg equation. This comparison includes the temporal profile and the speed of the LS demonstrating a very good agreement between the two models. Finally, we have derived a simple formula for the speed of the moving localized structures in the limit of a small third-order dispersion coefficient.

### ACKNOWLEDGMENTS

K.P. acknowledges the Methusalem foundation for financial support and the Fonds Wetenschappelijk Onderzoek-Vlaanderen under Project No. GOES819N. M.T. acknowledges support as a Research Director with the Fonds de la Recherche Scientifique F.R.S.-FNRS, Belgium. M.G.C. and M.F. acknowledge the financial support of the Millennium Institute for Research in Optics (Miro).

- [1] C. Markos, J. C. Travers, A. Abdolvand, B. J. Eggleton, and O. Bang, *Rev. Mod. Phys.* **89**, 045003 (2017).  
 [2] S. B. Cavalcanti, J. C. Cressoni, H. R. da Cruz, and A. S. Gouveia-Neto, *Phys. Rev. A* **43**, 6162 (1991);

- S. Pitois and G. Millot, *Opt. Commun.* **226**, 415 (2003);  
 J. D. Harvey, R. Leonhardt, S. Coen, G. Wong, J. C. Knight, W. J. Wadsworth, and P. St. J. Russell, *Opt. Lett.* **28**, 2225 (2003).

- [3] N. Y. Joly, F. G. Omenetto, A. Efimov, A. J. Taylor, J. C. Knight, and P. St. J. Russell, *Opt. Commun.* **248**, 281 (2005).
- [4] A. V. Yulin, D. V. Skryabin, and P. St. J. Russell, *Opt. Lett.* **29**, 2411 (2004); W. Wadsworth, N. Joly, J. Knight, T. Birks, F. Biancalana, and P. Russell, *Opt. Express* **12**, 299 (2004); A. Demircan and U. Bandelow, *Opt. Commun.* **244**, 181 (2005).
- [5] J. M. Dudley, G. Genty, and S. Coen, *Rev. Mod. Phys.* **78**, 1135 (2006); M. Kues, N. Brauckmann, T. Walbaum, P. Groß, and C. Fallnich, *Opt. Express* **17**, 15827 (2009).
- [6] L. A. Lugiato and R. Lefever, *Phys. Rev. Lett.* **58**, 2209 (1987).
- [7] A. J. Scroggie *et al.*, *Chaos Solitons Fractals* **4**, 1323 (1994).
- [8] F. Leo, S. Coen, P. Kockaert, S.-P. Gorza, P. Emplit, and M. Haelterman, *Nat. Photon.* **4**, 471 (2010).
- [9] T. J. Kippenberg, R. Holzwarth, and S. A. Diddams, *Science* **332**, 555 (2011); F. Ferdous, H. Miao, D. E. Leaird, K. Srinivasan, J. Wang, L. Chen, L. T. Varghese, and A. M. Weiner, *Nat. Photon.* **5**, 770 (2011); Y. K. Chembo and C. R. Menyuk, *Phys. Rev. A* **87**, 053852 (2013).
- [10] M. Tlidi, A. Mussot, E. Louvergneaux, G. Kozyreff, A. G. Vladimirov, and M. Taki, *Opt. Lett.* **32**, 662 (2007).
- [11] M. Tlidi and L. Gelens, *Opt. Lett.* **35**, 306 (2010).
- [12] M. Tlidi, L. Bahloul, L. Cherbi, A. Hariz, and S. Coulibaly, *Phys. Rev. A* **88**, 035802 (2013).
- [13] L. Bahloul, L. Cherbi, A. Hariz, and M. Tlidi, *Philos. Trans. R. Soc. A* **372**, 20140020 (2014).
- [14] S. Coen, M. Tlidi, P. Emplit, and M. Haelterman, *Phys. Rev. Lett.* **83**, 2328 (1999); P. Parra-Rivas, D. Gomila, and L. Gelens, *Phys. Rev. A* **95**, 053863 (2017); J. H. Talla Mbé, C. Milián, and Y. K. Chembo, *Eur. Phys. J. D* **71**, 196 (2017); P. Parra-Rivas, D. Gomila, M. A. Matias, and P. Colet, *Phys. Rev. Lett.* **110**, 064103 (2013); V. Odent, M. Tlidi, M. G. Clerc, P. Glorieux, and E. Louvergneaux, *Phys. Rev. A* **90**, 011806(R) (2014).
- [15] A. G. Vladimirov, S. V. Gurevich, and M. Tlidi, *Phys. Rev. A* **97**, 013816 (2018).
- [16] F. Biancalana, D. V. Skryabin, and P. S. J. Russell, *Phys. Rev. E* **68**, 046603 (2003).
- [17] F. Biancalana and D. V. Skryabin, *J. Opt. A: Pure Appl. Opt.* **6**, 301 (2004).
- [18] M. J. Schmidberger, D. Novoa, F. Biancalana, P. St. J. Russell, and N. Y. Joly, *Opt. Express* **22**, 3045 (2014).
- [19] G. P. Agrawal, *Nonlinear Fiber Optics, Optics and Photonics Series*, 2nd ed. (Academic Press, San Diego, 1995).
- [20] G. Kozyreff, M. Tlidi, A. Mussot, E. Louvergneaux, M. Taki, and A. G. Vladimirov, *Phys. Rev. Lett.* **102**, 043905 (2009).
- [21] J. Swift and P. C. Hohenberg, *Phys. Rev. A* **15**, 319 (1977).
- [22] M'F Hilali, G. Dewel, and P. Borckmans, *Phys. Lett. A* **217**, 263 (1996).
- [23] R. Lefever *et al.*, *J. Theor. Biol.* **261**, 194 (2009).
- [24] P. Mandel, *Theoretical Problems in Cavity Nonlinear Optics* (Cambridge University Press, Cambridge, UK, 1997).
- [25] K. Staliunas, *Phys. Rev. A* **48**, 1573 (1993); J. Lega, J. V. Moloney, and A. C. Newell, *Phys. Rev. Lett.* **73**, 2978 (1994); S. Longhi and A. Geraci, *Phys. Rev. A* **54**, 4581 (1996); M. Tlidi *et al.*, *Opt. Lett.* **25**, 487 (2000); S. Hache, C. R. Jones, and J. N. Kutz, *Opt. Commun.* **283**, 2588 (2010).
- [26] M. G. Clerc, A. Petrossian, and S. Residori, *Phys. Rev. E* **71**, 015205(R) (2005); C. Durniak, M. Taki, M. Tlidi, P. L. Ramazza, U. Bortolozzo, and G. Kozyreff, *ibid.* **72**, 026607 (2005); G. Kozyreff, S. J. Chapman, and M. Tlidi, *ibid.* **68**, 015201(R) (2003); G. Kozyreff and M. Tlidi, *Chaos* **17**, 037103 (2007); M. Tlidi *et al.*, *Lect. Notes Phys.* **751**, 381 (2008).
- [27] A. J. Alvarez-Socorro, M. G. Clerc, and M. Tlidi, *Chaos* **28**, 053119 (2018).
- [28] M. Tlidi, P. Mandel, and R. Lefever, *Phys. Rev. Lett.* **73**, 640 (1994); A. G. Vladimirov, R. Lefever, and M. Tlidi, *Phys. Rev. A* **84**, 043848 (2011).
- [29] M. Tlidi, M. Georgiou, and P. Mandel, *Phys. Rev. A* **48**, 4605 (1993); M. Tlidi and P. Mandel, *Chaos Solitons Fractals* **4**, 1475 (1994).
- [30] W. H. Press, B. P. Flannery, and S. A. Teukolsky, *TVW: Numerical Recipes in C: The Art of Scientific Computing* (Cambridge University Press, Cambridge, UK, 2002).
- [31] Y. Pomeau, *Physica D* **23**, 3 (1986).
- [32] M. Tlidi, A. G. Vladimirov, and P. Mandel, *IEEE J. Quantum Electron.* **39**, 216 (2003).
- [33] M. Tlidi, K. Staliunas, K. Panajotov, A. G. Vladimirov, and M. G. Clerc, *Philos. Trans. R. Soc. A* **372**, 20140101 (2014); L. Lugiato, F. Prati, and M. Brambilla, *Nonlinear Optical Systems* (Cambridge University Press, Cambridge, UK, 2015); Y. K. Chembo *et al.*, *Eur. Phys. J. D* **71**, 299 (2017); E. Meron, *Nonlinear Physics of Ecosystems* (CRC Press, Taylor & Francis Group, London, 2015); M. Tlidi, M. Clerc, and K. Panajotov, *Philos. Trans. R. Soc. A* **376**, 20140014 (2018).
- [34] K. Staliunas and V. Sanchez-Morcillo, *Transverse Patterns in Nonlinear Optical Resonators*, Springer Tracts in Modern Physics (Springer, Berlin, 2003); *Dissipative Solitons: from Optics to Biology and Medicine*, edited by N. Akhmediev and A. Ankiewicz, Lecture Notes in Physics Vol. 751 (Springer, New York, 2008); N. N. Rosanov, in *I. Transverse Patterns in Wide-aperture Nonlinear Optical Systems*, edited by E. Wolf, Progress in Optics Vol. 35 (Elsevier, Amsterdam, 1996), pp. 1–60; M. Tlidi, M. Taki, and T. Kolokolnikov, *Chaos* **17**, 037101 (2007); O. Descalzi, M. Clerc, S. Residori, and G. Assanto, *Localized States in Physics: Solitons and Patterns* (Springer Science & Business Media, New York, 2011); H. Leblond and D. Mihalache, *Phys. Rep.* **523**, 61 (2013); J. D. Murray, *Mathematical Biology, Biomathematics* Vol. 19 (Springer, Berlin, 1989).
- [35] D. A. C. Contreras and M. G. Clerc, *Phys. Rev. E* **91**, 032922 (2015).